An International Standard Formulation for *trans*-1-Chloro-3,3,3-trifluoroprop-1-ene [R1233zd(E)] Covering Temperatures from the Triple-point Temperature to 450 K and Pressures up to 100 MPa,

Ryo Akasaka[1, 2, a)] and Eric W. Lemmon[3]

[1)]*Department of Mechanical Engineering, Faculty of Science and Engineering, Kyushu Sangyo University, 2-3-1 Matsukadai, Higashi-ku, Fukuoka 8138503, Japan*

[2)]*Research Center for Next Generation Refrigerant Properties (NEXT-RP), International Institute for Carbon-Neutral Energy Research (WPI-I2CNER), Kyushu University, 744 Motooka, Nishi-ku, Fukuoka 8190395, Japan*

[3)]*Applied Chemicals and Materials Division, National Institute of Standards and Technology, 325 Broadway, Boulder, CO 80305, USA*

(Dated: 8 April 2022)

A new Helmholtz energy equation of state is presented for *trans*-1-chloro-3,3,3-trifluoroprop-1-ene [R1233zd(E)], which is expressed with temperature and density as the independent variables. Experimental data in the range of temperatures from 215 K to 444 K and pressures up to 35 MPa form the basis of the new equation. In this range, expected uncertainties ($k = 2$) of the new equation of state are 0.07 % for vapor pressures at temperatures above the normal boiling point temperature ($\approx$ 291 K), 0.2 % for vapor pressures at lower temperatures, 0.05 % for liquid densities, 0.15 % for vapor densities, 0.1 % for saturated liquid densities, 0.05 % for liquid-phase sound speeds, and 0.08 % for vapor-phase sound speeds. The new equation is valid at temperatures from the triple-point temperature (165.75 K) to 450 K and pressures up to 100 MPa with reasonable uncertainties outside the available range of data because it fully extrapolates with correct physical behavior to higher temperatures and pressures, and to lower temperatures. The equation of state presented here has been recommended as an international standard by the working group, presently revising ISO 17584 (Refrigerant Properties).

[a)]Electronic mail: ryo-a@ip.kyusan-u.ac.jp

CONTENTS

LIST OF TABLES

LIST OF FIGURES

List of Symbols

AAD	Average absolute deviation (%)
a	Molar Helmholtz energy (J mol^{-1})
B	Second virial coefficient (dm^3 mol^{-1})
C	Third virial coefficient (dm^6 mol^{-2})
c_p	Isobaric heat capacity (J mol^{-1} K^{-1})
c_v	Isochoric heat capacity (J mol^{-1} K^{-1})
D	Fourth virial coefficient (dm^9 mol^{-3})
d_i	Density exponent
e_i	Density exponent
F_i	Relative deviation in calculated value
h	Molar enthalpy (J mol^{-1})
k	Coverage factor
L_i	Penalty associated with the range of coefficients and exponents
M	Molar mass (g mol^{-1})
m_i	Coefficient (K)
N	Number of data points, number of atoms
n_i	Coefficient
P_i	Penalty associated with thermodynamic constraints
PIP	Phase identification parameter
p	Pressure (MPa)
R	Molar gas constant (8.314462618 J mol^{-1} K^{-1})
S	Objective function
S_1	Sum of the products of F_i and W_i
S_2	Sum of P_i
S_3	Sum of L_i
s	Molar entropy (J mol^{-1} K^{-1})
T	Temperature (K)
t_i	Temperature exponent
v	Molar volume (m^3 mol^{-1})
W_i	Weighting factor
w	Sound speed (m s^{-1})

Greek symbols

α	Dimensionless Helmholtz energy
β_i	Parameter in the Gaussian terms
γ_i	Parameter in the Gaussian terms
δ	Reduced density
ε_i	Parameter in the Gaussian terms
η_i	Parameter in the Gaussian terms
ρ	Density (mol dm^{-3})
τ	Reciprocal reduced temperature
ψ_i	Scaling factor for S_i
ω	Acentric factor

Superscripts

$\circ$	Ideal gas part
$'$	Saturated liquid
$''$	Saturated vapor
r	Residual part

Subscripts

0	Reference state
b	Normal boiling point
c	Critical point
calc	Calculated value
exp	Experimental value
tp	Triple point
s	Saturation

1. INTRODUCTION

1.1. Background

The substance *trans*-1-chloro-3,3,3-trifluoro-1-propene (CAS No. 102687-65-0), also known as R1233zd(E), is an unsaturated hydrochlorofluoroolefin (HCFO) and a fluorinated propene isomer. Due to its negligible ozone depletion potential (ODP), ultralow global warming potential (GWP), non-flammability, and favorable thermophysical properties, this refrigerant has been considered as a possible alternative to 2,2-dichloro-1,1,1-trifluoroethane (R123) and 1,1,1,3,3-pentafluoropropane (R245fa). Patten and Wuebbles[1] analytically determined the ODP as 0.00034, and IPCC AR5[2] reported the 100-year GWP as 1. Its ANSI/ASHRAE safety classification is "A1" (no flame propagation and no toxicity). R1233zd(E) was initially produced as a foam blowing agent, and later received much attention as a working fluid for centrifugal chillers, medium or high-temperature heat pumps, and organic Rankine cycles. Some manufacturers have already launched commercial chillers that use R1233zd(E).

Mondéjar *et al.*[3] first performed comprehensive property measurement for R1233zd(E) and obtained experimental data for the (p, ρ, T) behavior, vapor-phase sound speed, and vapor pressure. Based on these measurements, Mondéjar *et al.*[3] developed the first fundamental equation of state. With its availability in thermophysical property software, it has been extensively used in studies on this refrigerant. After the first equation of state was published, additional experimental data were reported for the liquid density (including those at saturation),[4–6] vapor density,[7] liquid-phase sound speed,[8,9] liquid isobaric heat capacity,[10] vapor-phase sound speed,[11] and vapor pressure.[4,7,12–14] The amount of these additional data is sufficient to update the first equation, and our new fitting techniques for developing reliable equations of state improve a number of characteristics in the equation. In collaboration with others,[15–21] we have improved our numerical algorithms for nonlinear optimization and found various thermodynamic constraints to help obtain reasonable extrapolation.

Recent measurements for R1233zd(E) were evaluated for their thermodynamic consistency, and only consistent datasets were employed in the development of the new equation. The state-of-the-art fitting techniques were applied in this work. The following sections discuss currently available experimental data, the functional form of the new equation, the fitting method employed, comparisons to the experimental data, and behavior in the critical and extrapolated regions. Fi-

nally, expected uncertainties in calculated properties with the new equation are summarized in the conclusions.

1.2. ISO17584

ISO17584 (Refrigerant Properties) tabulates the thermodynamic properties of commonly used refrigerants and refrigerant blends. The latest version ISO17584:2005[22] was published in 2005. Properties are provided for dichlorodifluoromethane (R12), chlorodifluoromethane (R22), difluoromethane (R32), 2,2-dichloro-1,1,1-trifluoroethane (R123), pentafluoroethane (R125), 1,1,1,2-tetrafluoroethane (R134a), 1,1,1-trifluoroethane (R143a), 1,1-difluoroethane (R152a), ammonia (R717), and carbon dioxide (R744), and the refrigerant blends R404A, R407C, R410A, and R507A. The following properties are included: density, pressure, internal energy, enthalpy, entropy, isobaric heat capacity, isochoric heat capacity, sound speed, and the Joule-Thomson coefficient, for both single phase states and along the liquid-vapor saturation boundaries.

To add recently developed low-GWP refrigerants to ISO17584, a scientific working group (ISO/TC 86/SC 8/WG 7) was organized in 2017 by experts in property measurement and modeling. The working group selected six refrigerants to be added: 2,3,3,3-tetrafluoroprop-1-ene (R1234yf), *trans*-1,3,3,3-tetrafluoroprop-1-ene [R1234ze(E)], *trans*-1-chloro-3,3,3-trifluoroprop-1-ene [R1233zd(E)], *cis*-1,1,1,4,4,4-hexafluorobut-2-ene [R1336mzz(Z)], propane (R290), and isobutane (R600a). The reason for this selection was the availability of experimental data covering wide ranges of temperature and pressure and an equation of state based on extensive experimental data. Subsequently, the working group evaluated equations of state available for these refrigerants and decided that the equation of state developed in this work should be used as an international standard formulation for R1233zd(E). The revised version ISO/DIS 17584 is now available as a Draft International Standard.[23]

2. AVAILABLE EXPERIMENTAL DATA

Table I summarizes the currently available experimental data for the thermodynamic properties of R1233zd(E) and their average absolute deviations (AADs) from calculated values with the new equation of state. The AAD in any property X is defined as

$$\mathrm{AAD}_X = \frac{100}{N_{\mathrm{exp}}} \sum_{i=1}^{N_{\mathrm{exp}}} \left| \frac{X_{i,\,\mathrm{exp}} - X_{i,\,\mathrm{calc}}}{X_{i,\,\mathrm{exp}}} \right|, \tag{1}$$

where N_{exp} is the number of data points in a dataset, $X_{i,\,\mathrm{exp}}$ is the ith experimental value, and $X_{i,\,\mathrm{calc}}$ is the calculated value at the state conditions as those of $X_{i,\,\mathrm{exp}}$. AADs in density measurements are shown for the (p, ρ, T) data. Although the new equation of state was fitted with selected experimental data, comparisons were made to all available experimental data, including those not used in the development of the equation. Figures 1 and 2 show the distributions of the experimental (p, ρ, T) and sound speed data, respectively, as well as the vapor pressure curve obtained from the new equation of state.

TABLE I. Available experimental data for R1233zd(E).

Author (year)	N	Range T (K)	Range p (MPa)	AAD (%)	Apparatus
		Vapor pressure			
Hulse *et al.* (2012)[24]	16	263–353		2.41	Isochoric method
Mondéjar *et al.* (2015)[3]	23	280–438		0.19	Two-sinker densimeter (static method)
Raabe (2015)[25]	8	273–383		4.57	Molecular simulation
Tanaka (2016)[4]	11	300–400		0.50	Extraction method
Di Nicola *et al.* (2017)[12]	32	293–353		0.15	VLE apparatus
Di Nicola *et al.* (2017)[12]	49	234–375		2.02	Isochoric method
Li *et al.* (2019)[13]	95	253–430		0.24	Burnett apparatus (experimental)
Li *et al.* (2019)[13]	95	253–430		0.42	Burnett apparatus (corrected)
Raabe (2020)[26]	7	273–283		5.17	Molecular simulation
Sakoda *et al.* (2020)[14]	12	300–410		0.03	Isochoric method
Yin *et al.* (2021)[7]	18	288–373		0.34	Burnett apparatus
		Saturated liquid density			
Hulse *et al.* (2012)[24]	13	243–293		0.15	Vibrating tube densimeter
Raabe (2015)[25]	8	273–383		0.20	Molecular simulation
Tanaka (2016)[4]	11	300–400		0.05	Extraction method
Raabe (2020)[26]	7	273–283		0.58	Molecular simulation
		Saturated vapor density			
Raabe (2015)[25]	8	273–383		3.88	Molecular simulation
Raabe (2020)[26]	7	273–283		4.56	Molecular simulation
		(p,ρ,T) *data*			
Mondéjar *et al.* (2015)[3] (liquid)	122	215–444	0.48–24.08	0.02	Two-sinker densimeter
Mondéjar *et al.* (2015)[3] (vapor)	43	350–440	0.26–1.92	0.06	Two-sinker densimeter
Tanaka (2016)[27]	97	328–444	0.78–9.77	3.12	Isochoric method
Romeo *et al.* (2017)[5]	30	274–333	1.00–25.01	0.02	Vibrating tube densimeter
Fedele *et al.* (2018)[6]	94	283–363	0.13–35.00	0.05	Vibrating tube densimeter
Fedele *et al.* (2018)[6]	60	308–373	0.17–0.69	0.26	Isochoric method
Yin *et al.* (2021)[7]	63	303–373	0.09–0.99	0.11	Burnett apparatus
		Isobaric heat capacity			
Liu and Zhao (2018)[10]	63	313–446	1.02–10.10	4.53	Flow calorimeter
		Sound speed			
Mondéjar *et al.* (2015)[3]	155	290–420	0.07–2.07	0.09	Spherical resonator
Lago *et al.* (2018)[8]	41	273–353	0.17–35.06	0.39	Dual-path pulse-echo
McLinden and Perkins (2022)[9]	133	230–420	0.13–25.61	0.05	Dual-path pulse-echo
Kano *et al.* (2020)[11]	36	313–403	0.03–0.89	0.06	Cylindrical resonator

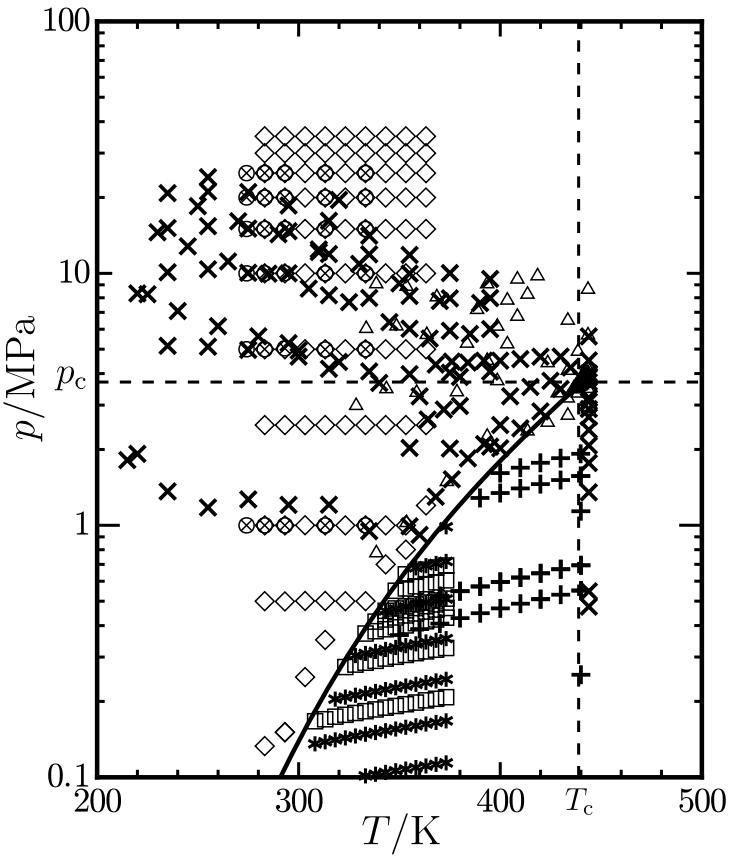

FIG. 1. Distribution of experimental (p, ρ, T) data for R1233zd(E): ($\times$) Mondéjar *et al.*[3] (liquid and supercritical); ($+$) Mondéjar *et al.*[3] (vapor); ($\triangle$) Tanaka;[27] ($\otimes$) Romeo *et al.*;[5] ($\diamond$) Fedele *et al.*[6] (liquid); ($\square$) Fedele *et al.*[6] (vapor); ($*$) Yin *et al.*[7]

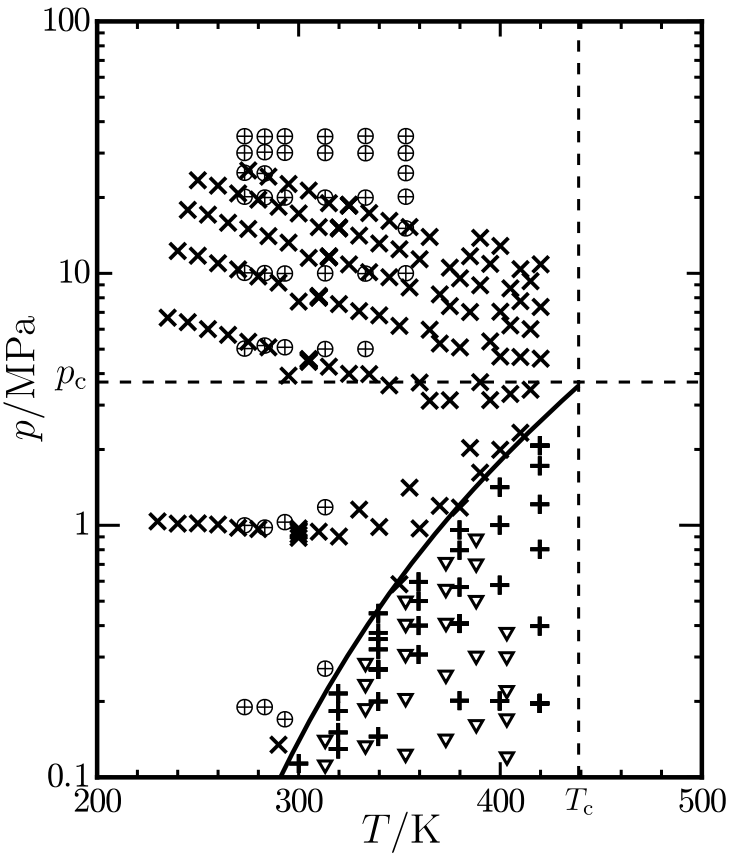

FIG. 2. Distribution of experimental sound-speed data for R1233zd(E): (+) Mondéjar *et al.*[3] (vapor); (⊕) Lago *et al.*[8] (liquid); (×) McLinden and Perkins[9] (liquid); (▽) Kano *et al.*[11] (vapor).

3. FUNDAMENTAL EQUATION OF STATE

3.1. Critical parameters and other fundamental constants

Table II summarizes the available data for the critical parameters of R1233zd(E). Hulse *et al.*[24] first measured the critical temperature by visual observation of the disappearance and reappearance of the meniscus, and then determined the critical pressure with extrapolation of a vapor pressure correlation. Mondéjar *et al.*[3] determined the critical temperature and density while fitting the first equation of state. The resulting critical temperature is 0.85 K higher than the value measured by Hulse *et al.*[24] Tanaka and Akasaka[28] measured the critical temperature, pressure, and density by visual observation coupled with image processing. Their critical temperature is similar to the value of Hulse *et al.*[24]

Accurate values for the critical parameters, particularly, the critical temperature, are essential for the formulation of reliable equations of state since they are often used as the reducing parameters for the independent variables. In this work, the critical temperature of Tanaka and Akasaka[28] (438.86 K) was adopted as the reducing temperature because this is most consistent with the experimental data for the vapor pressure and (p, ρ, T) behavior. Generally, experimental critical densities involve uncertainties larger than those in critical temperatures due to the infinite compressibility at the critical point and the difficulty of reaching thermodynamic equilibrium; therefore, this work used the critical density of Tanaka and Akasaka[28] ($\approx$ 3.592 mol dm^{-3}) as an initial value of the reducing density, and then further adjusted it during the fitting of the new equation. This adjustment improved the representation of the vapor pressure and (p, ρ, T) behavior. The final value of the critical density was 3.704 mol dm^{-3}. The critical pressure is calculated from the new equation of state as 3.5828 MPa at 438.86 K and 3.704 mol dm^{-3}. Tomassetti *et al.*[29] measured the triple-point temperature of R1233zd(E) as 165.75 K. This work regards this value as the lower temperature limit of the applicable range of the new equation, where the vapor pressure is calculated as 8.628 Pa.

Table III lists fixed-point constants of R1233zd(E), including the critical parameters and other characteristic properties calculated from the new equation of state.

TABLE II. Available data for the critical parameters for R1233zd(E).

Author (year)	T_c (K)	p_c (MPa)	ρ_c	Remarks
Hulse *et al.* (2012)[24]	438.75	3.7721	–	Visual observation
Mondéjar *et al.* (2015)[3]	439.6	3.6237	3.68 mol dm^{-3}	Fitted parameters
Tanaka and Akasaka (2021)[28]	438.86	3.5575	486.7 kg m^{-3} (≈ 3.592 mol dm^{-3})	Visual observation
This work	438.86	3.5828	3.704 mol dm^{-3}	

TABLE III. Fixed-point constants and other characteristic properties of R1233zd(E)[a].

Property	Symbol	Value
CAS number		102687-65-0
Chemical formula		$CF_3CH{=}CHCl$
Molar mass	M	130.4962 g mol^{-1}
Critical temperature	T_c	438.86 K
Critical pressure	p_c	3.5828 MPa
Critical density	ρ_c	3.704 mol dm^{-3}
Triple-point temperature	T_{tp}	165.75 K
Triple-point pressure	p_{tp}	8.628 Pa
Saturated liquid density at triple point	ρ'_{tp}	11.85 mol dm^{-3}
Saturated vapor density at triple point	ρ''_{tp}	6.261×10^{-6} mol dm^{-3}
Normal boiling point temperature	T_b	291.28 K
Saturated liquid density at normal boiling point	ρ'_b	9.804 mol dm^{-3}
Saturated vapor density at normal boiling point	ρ''_b	0.04364 mol dm^{-3}
Reference temperature for ideal gas properties	T_0	273.15 K
Reference pressure for ideal gas properties	p_0	0.001 MPa
Reference ideal-gas enthalpy at T_0	h°_0	52752.273510 J mol^{-1}
Reference ideal-gas entropy at T_0 and p_0	s°_0	260.14966456 J mol^{-1} K^{-1}
Acentric factor	ω	0.304

[a] All properties in this table were determined in this work except M, T_c, and T_{tp}.

3.2. Equation of state

3.2.1. Overview

The new equation of state for R1233zd(E) is expressed in terms of the Helmholtz energy with independent variables of temperature and density. The equation of state has the form:

$$\frac{a(T,\rho)}{RT} = \alpha(\tau,\delta) = \alpha^{\circ}(\tau,\delta) + \alpha^{\mathrm{r}}(\tau,\delta), \tag{2}$$

where a is the molar Helmholtz energy, α is the dimensionless Helmholtz energy, $R = 8.314462618$ J mol^{-1} K^{-1} is the molar gas constant, $\tau = T_{\mathrm{c}}/T$ is the reciprocal reduced temperature, and $\delta = \rho/\rho_{\mathrm{c}}$ is the reduced density. The value of R is a slightly rounded value of the exact value[30] (differing by about 18 parts per trillion). The dimensionless Helmholtz energy α is split into an ideal-gas part α° expressing ideal-gas properties and a residual part α^{r} corresponding to the macroscopic influence of intermolecular forces between molecules. As demonstrated in the following sections, α° and α^{r} are individually formulated.

Since Eq. (2) is one of the four fundamental equations, all single-phase thermodynamic properties can be calculated from derivatives of Eq. (2) with respect to temperature and density. For example, equations for calculating compressibility factor Z, molar enthalpy h, isochoric heat capacity c_v, and sound speed w are

$$Z = \frac{p}{\rho RT} = 1 + \delta\left(\frac{\partial\alpha^{\mathrm{r}}}{\partial\delta}\right)_{\tau}, \tag{3}$$

$$\frac{h}{RT} = \tau\left[\left(\frac{\partial\alpha^{\circ}}{\partial\tau}\right)_{\delta} + \left(\frac{\partial\alpha^{\mathrm{r}}}{\partial\tau}\right)_{\delta}\right] + \delta\left(\frac{\partial\alpha^{\mathrm{r}}}{\partial\delta}\right)_{\tau} + 1, \tag{4}$$

$$\frac{c_v}{R} = -\tau^2\left[\left(\frac{\partial^2\alpha^{\circ}}{\partial\tau^2}\right)_{\delta} + \left(\frac{\partial^2\alpha^{\mathrm{r}}}{\partial\tau^2}\right)_{\delta}\right], \text{ and} \tag{5}$$

$$\frac{w^2 M}{RT} = 1 + 2\delta\left(\frac{\partial\alpha^{\mathrm{r}}}{\partial\delta}\right)_{\tau} + \delta^2\left(\frac{\partial^2\alpha^{\mathrm{r}}}{\partial\delta^2}\right)_{\tau} - \frac{\left[1 + \delta\left(\frac{\partial\alpha^{\mathrm{r}}}{\partial\delta}\right)_{\tau} - \delta\tau\frac{\partial^2\alpha^{\mathrm{r}}}{\partial\delta\partial\tau}\right]^2}{\tau^2\left[\left(\frac{\partial^2\alpha^{\circ}}{\partial\tau^2}\right)_{\delta} + \left(\frac{\partial^2\alpha^{\mathrm{r}}}{\partial\tau^2}\right)_{\delta}\right]}. \tag{6}$$

The location of the saturation boundaries requires an iterative solution of the physical constraints on saturation (Maxwell criteria); specifically, the following two equations are satisfied on saturation at a given temperature T:

$$p(T,\rho') = p(T,\rho'') \tag{7}$$

and

$$g(T,\rho') = g(T,\rho''), \tag{8}$$

where g is the molar Gibbs energy and calculated as

$$\frac{g}{RT} = 1 + \alpha^\circ + \alpha^\mathrm{r} + \delta\left(\frac{\partial\alpha^\mathrm{r}}{\partial\delta}\right)_\tau. \tag{9}$$

Kretzschmar *et al.*,[31] Span,[32] and Akasaka[33] discuss robust numerical algorithms to obtain the Maxwell solutions correctly.

3.2.2. Ideal-gas Helmholtz energy

The ideal-gas Helmholtz energy α° is analytically obtained from an equation for the isobaric heat capacity of the ideal gas (c_p°) according to the following equation:

$$\alpha^\circ(\tau,\delta) = \frac{h_0^\circ\tau}{RT_\mathrm{c}} - \frac{s_0^\circ}{R} - 1 + \ln\frac{\delta\tau_0}{\delta_0\tau} - \frac{\tau}{R}\int_{\tau_0}^{\tau}\frac{c_p^\circ}{\tau^2}\mathrm{d}\tau + \frac{1}{R}\int_{\tau_0}^{\tau}\frac{c_p^\circ}{\tau}\mathrm{d}\tau, \tag{10}$$

where $\tau_0 = T_\mathrm{c}/T_0$, $\delta_0 = \rho_0/\rho_\mathrm{c} = p_0/(RT_0\rho_\mathrm{c})$, T_0 is the temperature at a reference state, p_0 is a reference pressure for the ideal-gas properties, and ρ_0 is the ideal-gas density at T_0 and p_0. This work used the Planck-Einstein form to express the c_p° equation, which has the form

$$\frac{c_p^\circ}{R} = n_0^\circ + \sum_{i=1}^{2} n_i^\circ\left(\frac{m_i^\circ}{T}\right)^2\frac{\exp(m_i^\circ/T)}{[\exp(m_i^\circ/T)-1]^2}. \tag{11}$$

The value of n_0° is theoretically always four for nonlinear polyatomic molecules to account for all but the vibrational contributions to the ideal-gas isochoric heat capacity c_v° as given by

$$\begin{aligned} n_0^\circ &= \frac{(c_v^\circ)_\mathrm{translation}}{R} + \frac{(c_v^\circ)_\mathrm{rotation}}{R} + \frac{c_p^\circ - c_v^\circ}{R} \\ &= \frac{3}{2} + \frac{3}{2} + 1 \\ &= 4. \end{aligned} \tag{12}$$

The summation on the right-hand side of Eq. (11) represents the vibrational contribution to c_v°. Generally, nonlinear polyatomic molecules consisting of N atoms have $(3N - 6)$ vibrational modes.[34] The R1233zd(E) molecule (consisting of nine atoms) has 21 vibrational modes, and the contribution of each mode attains the value of R at extremely high temperature; therefore, the value of c_p°/R approaches 25 (without considering the effect of anharmonicity) at extremely high temperatures. The molecule will dissociate before this limit is relevant, but the correct extrapolation is vital for the formulation of reliable equations of state.

Values of c_p° are experimentally determined from vapor-phase sound speed data or analytically estimated from quantum analyses. Kano[35] experimentally obtained c_p° values from vapor-phase sound speed data. Hulse *et al.*[24] presented c_p° values calculated with Gaussian 09,[36] where the scaling factor by Irikura *et al.*[37] was used for the frequencies. In this work, the coefficients n_i° and m_i° in Eq. (11) were initially determined by fitting the c_p° values of Kano,[35] and then further adjusted during the fitting of the residual part to obtain better agreement with sound speed data for both the liquid and vapor phases. The final values of n_i° and m_i° are given in Table IV.

TABLE IV. Coefficients of Eq. (11).

i	n_i°	m_i° (K)
0	4.0	
1	13.7	761
2	7.0974	2870
3	−17.291229931888	
4	10.404947446884	

Applying Eq. (11) to Eq. (10), the following expression for the ideal-gas Helmholtz energy is obtained:

$$\alpha^\circ(\tau,\delta) = \ln\delta + n_3^\circ + n_4^\circ\tau + (n_0^\circ - 1)\ln\tau + \sum_{i=1}^{2} n_i^\circ \ln\left[1 - \exp\left(-\frac{m_i^\circ \tau}{T_c}\right)\right], \tag{13}$$

where values of n_3° and n_4°, which are also given in Table IV, were determined so that the specific enthalpy and entropy of the saturated liquid state at 0 ℃ are 200 kJ kg^{-1} and 1 kJ kg^{-1} K^{-1}, respectively, corresponding to the common convention of the refrigeration industry. Table IV gives additional digits for n_3° and n_4° beyond those required to obtain the expected uncertainties in order to reproduce the enthalpy and entropy values specified for the saturated liquid at 0 ℃ to within machine precision.

3.2.3. Residual Helmholtz energy

The functional form for the residual Helmholtz energy was empirically determined by fitting experimental data. According to recent developments of Helmholtz energy equations of state for

refrigerants, this work used the functional form:

$$\alpha^{\mathrm{r}}(\tau,\delta) = \sum n_i \tau^{t_i} \delta^{d_i} + \sum n_i \tau^{t_i} \delta^{d_i} \exp(-\delta^{e_i}) + \sum n_i \tau^{t_i} \delta^{d_i} \exp\left[-\eta_i(\delta-\varepsilon_i)^2 - \beta_i(\tau-\gamma_i)^2\right], \tag{14}$$

where the first, second, and final summations are called polynomial, exponential, and Gaussian bell-shaped (or simply Gaussian) terms, respectively. The values of t_i should be greater than zero to avoid numerical instability at very high temperatures, and d_i and e_i should be integers greater than zero so that the contributions from all virial coefficients vanish at zero density.

The polynomial and exponential terms form the basis of the corresponding states principle, and most equations of state recently developed for hydrofluoroolefin (HFO) and hydrochlorofluoroolefin (HCFO) refrigerants employ five polynomial terms and five exponential terms with similar coefficients and exponents. The Gaussian terms, on the other hand, are used to model the properties of each fluid more accurately, and their coefficients, exponents, and number of the terms are quite different between fluids. Four or five Gaussian terms are typically necessary for HFO and HCFO refrigerants with limited experimental data. For those with sufficient available data, additional Gaussian terms are employed for more accurate modeling. The new equation for R1233zd(E) uses eight Gaussian terms for the residual part.

Various thermodynamic properties can be used during fitting, including densities, vapor pressures, critical parameters, sound speeds, virial coefficients, and heat capacities. Density and sound speed data are essential in the development of accurate equations of state because experimental uncertainties in these properties are normally smaller than those in other properties. In addition to uncertainties, thermodynamic consistency between data used while fitting is crucial. The consistency between available experimental data was first examined before all else, and inconsistent data were excluded. For the reduction of computation time, fitting was carried out with a subset of consistent experimental datasets, which were chosen to cover the full range of experimental conditions; comparisons were then made to the full data points.

Lemmon and Jacobsen[38] initially presented the methods used in the nonlinear least-squares fitting algorithm to obtain reliable equations of state, and subsequently correlators have advanced it during the last decade, e.g., Lemmon *et al.*,[15] Thol *et al.*,[16] Akasaka *et al.*,[17] Thol and Lemmon,[18] Gao *et al.*,[19] Herrig *et al.*,[20] and Akasaka and Lemmon.[21] The most recent fitting techniques used in this work are summarized here.

The objective function (S) used while fitting consists of three sums as follows:

$$S = \psi_1 S_1 + \psi_2 S_2 + \psi_3 S_3, \tag{15}$$

where

$$S_1 = \sum W_{p,i} F_{p,i}^2 + \sum W_{\rho,i} F_{\rho,i}^2 + \sum W_{w,i} F_{w,i}^2 + \cdots, \tag{16}$$

$$S_2 = \sum P_i, \tag{17}$$

and

$$S_3 = \sum L_i. \tag{18}$$

The sums S_1, S_2, and S_3 are based on the sum of squared deviations in experimental properties from calculated values (F_i^2), the sum of penalties added to keep the equation within certain thermodynamic constraints (P_i), and the sum of penalties added to keep the coefficients and exponents of the equation within appropriate ranges (L_i), and ψ_1, ψ_2, and ψ_3 are their scaling factors.

Deviations in pressure F_p, in density F_ρ, and in sound speed F_w were calculated as

$$F_p = \frac{p_{\text{exp}} - p_{\text{calc}}}{p_{\text{exp}}}, \tag{19}$$

$$F_\rho = \frac{p_{\text{exp}} - p_{\text{calc}}}{\rho_{\text{exp}}} \left(\frac{\partial \rho}{\partial p} \right)_T, \tag{20}$$

and

$$F_w = \frac{w_{\text{exp}} - w_{\text{calc}}}{w_{\text{exp}}}, \tag{21}$$

where the subscripts exp and calc indicate experimental and calculated values. The pressure deviation F_p is often used for (p, ρ, T) data in the vapor phase and critical region, and the density deviation F_ρ is applied to liquid-phase (p, ρ, T) data. The derivative $(\partial \rho / \partial p)_T$ in Eq. (20) is used to avoid iterative calculations to obtain density at a given pressure and temperature. Deviations for other experimental data are calculated in the same manner as the sound speed deviation F_w given in Eq. (21). The i^{th} data point is individually weighted by weighting factors W_i, which were determined according to type, region, and experimental uncertainty. Typical weighting factors used in this work were 1 for saturated liquid and vapor densities and ideal-gas isobaric heat capacities, 10 to 10^2 for vapor pressures and vapor densities, 10^2 to 10^4 for liquid densities, and 10^3 to 10^4 for sound speeds. Substantial weighting factors were sometimes given to vapor pressure data if they were very consistent with (p, ρ, T) and sound speed data.

Various thermodynamic constraints were applied to the fitting to ensure that the equation of state was well behaved near the critical point and would reliably extrapolate beyond the range of the experimental data. Span and Wagner,[39] Lemmon and Jacobsen,[38] and Lemmon *et al.*[15] discuss these constraints in detail. Akasaka and Lemmon[21] describe physically correct behavior of the critical isotherm, virial coefficients, rectilinear diameter, and phase identification parameter (PIP),[40] which are the essential primary constraints. If the equation violated the i^{th} constraint, then a penalty P_i was added to S_2. Values of P_i changed gradually depending on how much a constraint was violated. For some primary constraints, such as those related to the critical isotherm and virial coefficients, large weighting factors were applied so that the penalties would be larger than those for the experimental data; this forced the equation to always obey these constraints. If the equation completely fulfilled all constraints, then S_2 would approach zero.

The final sum S_3 relates to the adjustable ranges of the coefficients n_i, the temperature exponents t_i, and the Gaussian parameters η_i, ε_i, β_i, and γ_i. Although they are arbitrary in nature, recent studies[18–21] found suitable ranges for which equations of state behave well over wide ranges of temperatures and pressures. In this work, for example, the Gaussian parameters except the last two terms (17^{th} and 18^{th}) were kept within the following ranges while fitting:

$$0.4 \leq \eta_i \leq 3, \tag{22}$$

$$0.2 \leq \varepsilon_i \leq 1.4, \tag{23}$$

$$0.3 \leq \beta_i \leq 3, \text{ and} \tag{24}$$

$$0.6 \leq \gamma_i \leq 2.4. \tag{25}$$

A penalty L_i was added to S_3 when the parameters approached their upper or lower boundaries given by Eqs. (22)–(25), even if they were still within these ranges. The value of L_i increased rapidly when the parameters exceeded the boundaries. This process forced the parameters to always remain within the suitable ranges.

The last two Gaussian terms, which have positive and negative contributions with very similar magnitude, were used to model the critical region. Differences between these contributions become significant while approaching the critical point. These terms were first introduced by Herrig *et al.*[20] to the equation of state for heavy water. Akasaka *et al.*[41] used similar terms in the equation for trifluoroethene (R1123). An example is shown below that demonstrates the effect of these terms on the modeling of the isochoric heat capacity.

The scaling factors ψ_1, ψ_2, and ψ_3 are used to change the contributions of S_1, S_2, and S_3 to the objective function S. Initially, larger values were given to ψ_2 and ψ_3 rather than ψ_1 to roughly fix the functional form. Once S_2 and S_3 had become sufficiently small, the value of ψ_1 was gradually increased until consistent experimental data were adequately represented.

The final values of the coefficients and exponents in Eq. (14) are given in Table V. The large number of digits for n_3 and n_4 are required to exactly represent the critical point.

TABLE V. Coefficients and exponents of Eq. (14) for R1233zd(E).

i	n_i	t_i	d_i	e_i	η_i	β_i	γ_i	ε_i
1	0.04394257	1.0	4					
2	1.062919	0.182	1					
3	−1.2879140374971	0.865	1					
4	−0.8088618920845	1.0924	2					
5	0.2372427	0.49	3					
6	−1.9403	1.958	1	2				
7	−2.831967	2.05	3	2				
8	0.373421	0.658	2	1				
9	−1.515798	2.051	2	2				
10	−0.02755627	0.862	7	1				
11	4.24023	1.852	1		1.532	0.2912	1.7171	0.8834
12	−0.03152671	1.92	2		0.635	0.6245	0.63	1.386
13	−1.366494	1.936	3		1.4056	0.669	0.7852	0.5196
14	2.647143	1.515	1		1.451	0.5798	2.251	1.133
15	−2.325463	2.668	1		1.395	0.4643	1.821	0.9788
16	−0.2541521	1.755	1		2.259	2.449	2.074	1.166
17	0.1330834	0.526	1		24.3	1061.4	1.0797	0.9244
18	−0.1569217	2.98	1		23.6	917.8	1.084	0.9372

3.3. Comparisons to experimental data

Deviations in experimental data from calculated values with the new equation of state were statistically evaluated mainly by averaged values of the relative deviations defined in Eq. (1). For the vapor pressures, absolute differences between experimental and calculated values are sometimes evaluated because relative uncertainties in vapor pressure measurements are often larger at very low pressures (near the triple point).

3.3.1. Vapor pressure data

Figure 3 shows plots of relative deviations and differences in experimental vapor pressures versus temperature. Table I includes the molecular simulation results[25,26] for comparison, but they do not appear in these plots because they are off-scale in most cases. The vapor pressure data of Hulse *et al.*[24] have significant uncertainties, probably due to low sample purity used in their measurement. Excluding the simulation results[25,26] and the data of Hulse *et al.*[24] gives a total of 317 data available for vapor pressure, and the overall average deviation and difference from calculated values with the new equation of state are 0.56 % and 1.59 kPa. For the data at temperatures above the normal boiling point (291.28 K), where 268 data points are included, the average deviation decreases to 0.18 %.

The data of Sakoda *et al.*[14] are represented within 0.067 %; the average deviation is 0.027 %. Although the difference at the highest temperature (410 K) is particularly large (−1.45 kPa), differences in other data points are less than 0.6 kPa, which is within their experimental uncertainty (1 kPa). Systematic negative deviations are observed in the data of Mondéjar *et al.*,[3] except one data point at the lowest temperature (280.009 K). Their average deviation is 0.19 %, which would be acceptable in most engineering applications; however, deviations in the data at temperatures above 320 K are larger than the experimental uncertainties (0.022 to 0.030 %). Di Nicola *et al.*[12] presented two datasets, each measured with a different apparatus. The datasets show systematic positive deviations from the equation of state. Differences in the data measured with the isochoric method are always about 1 kPa, and their relative deviations become more substantial as the temperature decreases. The data measured with the VLE apparatus show smaller deviations than those with the isochoric method, and exhibit a similar trend to the data of Sakoda *et al.*[14] at temperatures below 350 K. Li *et al.*[13] also reported two datasets; one includes experimental values without any

corrections, and the other includes values corrected taking the sample purity into account. The data without corrections show a similar trend to the data of Sakoda *et al.*[14] They are represented within 0.1 % at temperatures from 300 K to 400 K, where the differences are almost within their experimental uncertainties (0.33 to 1.18 kPa). At higher temperatures, larger relative deviations of up to 0.2 % are observed. Larger deviations are also observed at temperatures below 300 K, but the uncertainties in the data in this range are higher (1.9 % at the lowest temperature) due to the very low vapor pressures (less than atmospheric pressure). The trend of the data with corrections, on the other hand, is similar to the data of Mondéjar *et al.*,[3] and systematic negative deviations down to −0.2 % are observed.

Figure 4 depicts differences in the saturation temperatures as a function of pressure; this plot is particularly applicable for heat transfer calculations where the saturation temperature is calculated based on a measured pressure in a heat exchanger. Differences in calculated saturation temperatures from experimental values are almost within 0.1 K.

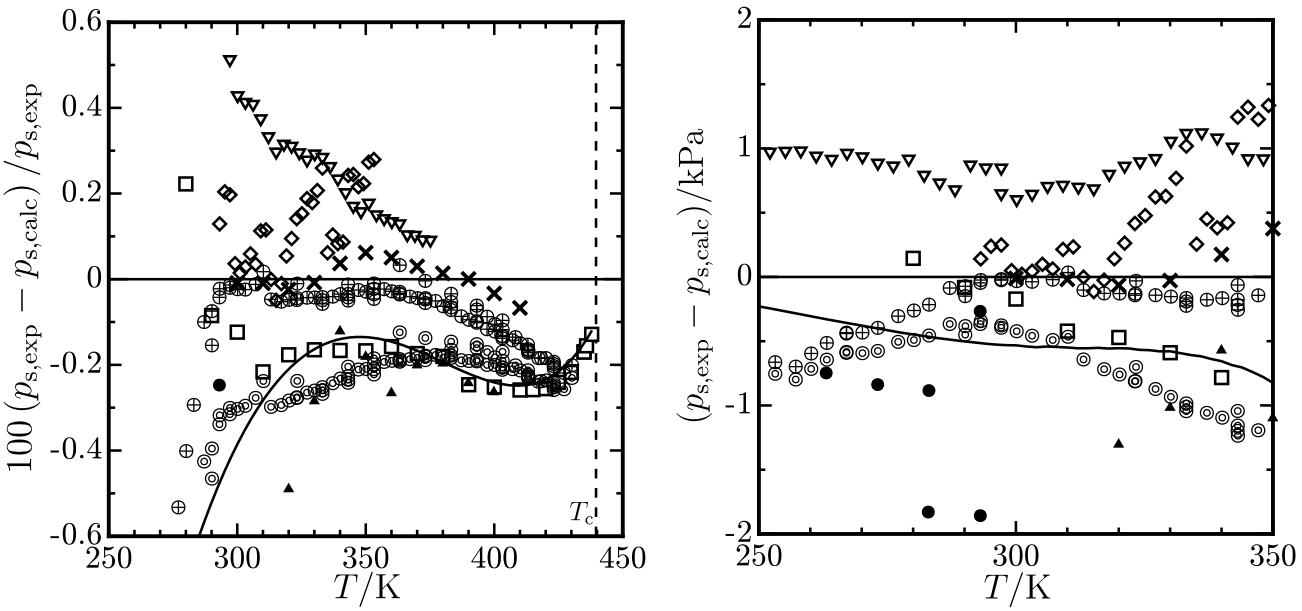

(a) (b)

FIG. 3. Relative deviations (a) and differences (b) in experimental vapor pressures of R1233zd(E) from calculated values with the new equation of state: (●) Hulse *et al.*;[24] (□) Mondéjar *et al.*[3] (experimental); (—) Mondéjar *et al.*[3] (equation of state); (▲) Tanaka;[4] (◇) Di Nicola *et al.*[12] (VLE apparatus); (▽) Di Nicola *et al.*[12] (isochoric method); (⊕) Li *et al.*[13] (experimental); (◎) Li *et al.*[13] (corrected); (×) Sakoda *et al.*[14]

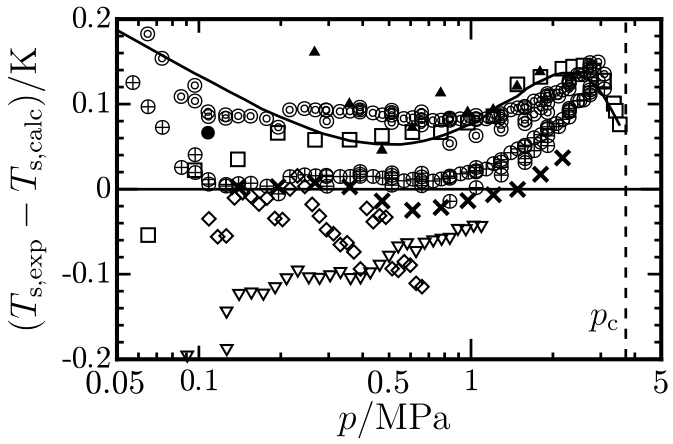

FIG. 4. Differences in experimental and calculated saturation temperatures of R1233zd(E): (●) Hulse *et al.*;[24] (□) Mondéjar *et al.*[3] (experimental); (—) Mondéjar *et al.*[3] (equation of state); (▲) Tanaka;[4] (◇) Di Nicola *et al.*[12] (VLE apparatus); (▽) Di Nicola *et al.*[12] (isochoric method); (⊕) Li *et al.*[13] (experimental); (◎) Li *et al.*[13] (corrected); (×) Sakoda *et al.*[14]

3.3.2. (p, ρ, T) *data*

Deviations in density are discussed here. For the liquid and supercritical regions, three datasets (Mondéjar *et al.*,[3] Romeo *et al.*,[5] and Fedele *et al.*[6]) are available. They are mostly consistent with each other. A total of 246 data points are available in these datasets, and the overall average deviation from calculated values with the new equation of state is 0.034 %. Figure 5 shows plots of relative deviations versus pressure in different temperature intervals. The average deviation in the data of Mondéjar *et al.*[3] is 0.021 %; this slightly exceeds their typical experimental uncertainties (0.011–0.015 %). Several data points near the critical point show larger deviations up to 0.12 %. These deviations, however, are less than typical uncertainties in calculated densities in the critical region. Densities in the (p, ρ, T) data of Fedele *et al.*[6] are represented with an average deviation of 0.054 %. Fedele *et al.*[6] reported the expanded uncertainty in their density measurements as 0.8 kg m^{-3}, which corresponds to relative uncertainties from 0.058 % to 0.072 %. Most data points are represented within the uncertainty. Some data at pressures above 15 MPa at the highest temperature (363.15 K) show larger deviations up to 0.11 %. Densities in the (p, ρ, T) data of Romeo *et al.*[5] are also accurately represented, where the maximum and average deviations are 0.053 % and 0.022 %. The maximum deviation is less than the experimental uncertainty claimed by the authors (0.07 %), and the average deviation is similar to that in the data of Mondéjar *et al.*[3]

For the vapor phase, four datasets (Mondéjar *et al.*,[3] Tanaka,[27] Fedele *et al.*,[6] and Yin *et al.*[7]) are available. Figure 6 shows plots of relative deviations in these data versus temperature or pressure. The datasets other than Tanaka[27] are nearly consistent; their deviations are normally within 0.4 %, except for some data points of Fedele *et al.*[6] For a total of 166 data points in these three datasets, the overall average deviation is 0.15 %. The data of Tanaka[27] show systematic positive deviations, which often exceed 0.4 %; therefore, they were excluded from the overall statistical analysis of vapor density deviations. The data of Mondéjar *et al.*[3] are represented within 0.2 %, and the average deviation is 0.058 %. Although this average deviation is larger than typical experimental uncertainties in the data (0.012–0.025 %), it is quite acceptable in engineering applications. Deviations in the data of Fedele *et al.*[6] are scattered between −0.36 % and 0.83 %, and their average deviation is 0.26 %. Fedele *et al.*[6] evaluated the experimental uncertainty in the specific volume as 0.00013 m^3 kg^{-1}; this corresponds to relative uncertainties in density from 0.12 % to 0.44 %. Most data points are represented within the uncertainties. Along each isochore, larger deviations of up to 0.83 % are observed at the lowest temperature, where uncertainties are generally larger

than those evaluated by the author due to their proximity to saturation. Deviations in the data of Yin *et al.*[7] are consistent with the data of Mondéjar *et al.*[3] and less scattered than those of Fedele *et al.*,[6] which are observed almost within 0.2 %. The average deviation is 0.11 %; this is similar to the experimental uncertainty (0.1 %). Larger deviations up to 0.40 % are sometimes observed at temperatures below 330 K.

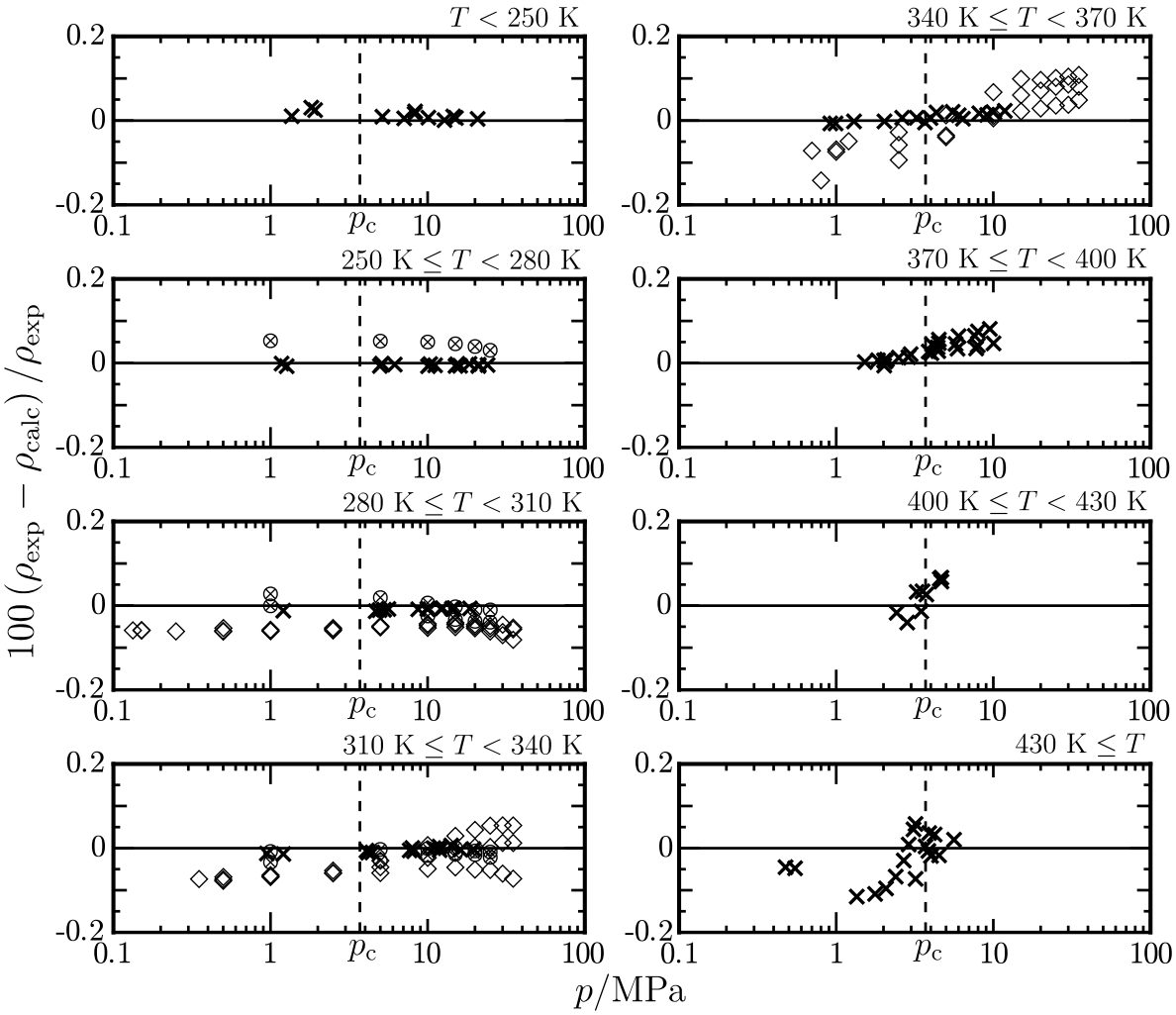

FIG. 5. Relative deviations in the experimental liquid and supercritical densities of R1233zd(E): (×) Mondéjar *et al.*;[3] (⊗) Romeo *et al.*;[5] (◇) Fedele *et al.*[6]

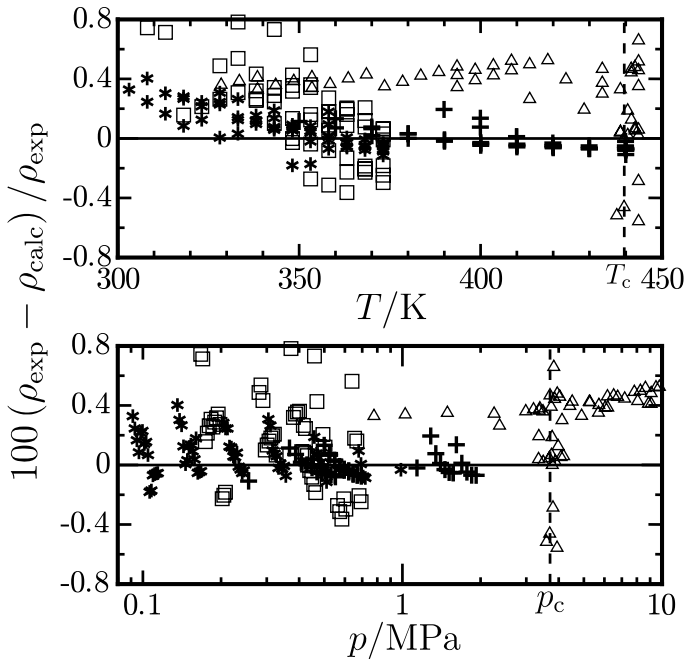

FIG. 6. Relative deviations in the experimental vapor densities for R1233zd(E): (+) Mondéjar *et al.*;[3] (△) Tanaka;[27] (□) Fedele *et al.*;[6] (∗) Yin *et al.*[7]

3.3.3. Saturated liquid density data

Hulse *et al.*[24] and Tanaka[4] measured the saturated liquid densities with different approaches. Figure 7 shows their relative deviations. Although the fitting did not incorporate these data, they reasonably correspond to calculated values with the new equation; this means that the two datasets shown here are consistent with the vapor pressure and (p, ρ, T) data to which the equation was fitted. Systematic negative deviations are observed in the data of Hulse *et al.*,[24] except one data point at 255.66 K. Their average deviation is 0.15 %; this is acceptable in most engineering applications. The data of Tanaka[4] are represented within 0.11 %; the average deviation is 0.054 %. The experimental uncertainties estimated by the author are 0.9 to 1.4 kg m^{-3}, and this is equivalent to a relative uncertainty of 0.080 to 0.14 %.

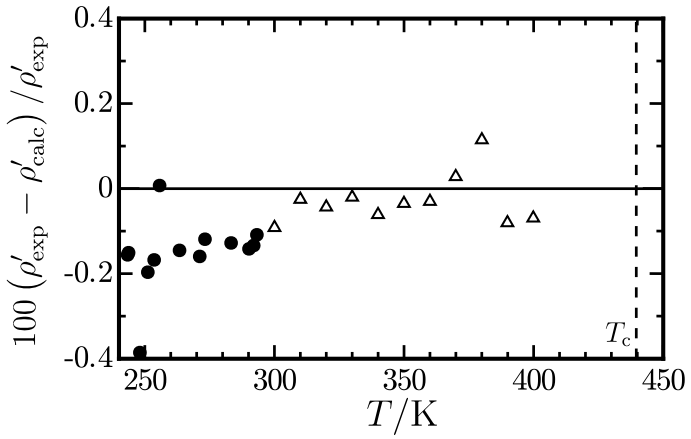

FIG. 7. Relative deviations in experimental data for the saturated liquid density of R1233zd(E): (●) Hulse *et al.*;[24] (△) Tanaka.[4]

3.3.4. Caloric data

Figure 8 shows plots of relative deviations in experimental sound-speed data versus pressure in different temperature intervals. Among the liquid-phase sound speeds, significant discrepancy is observed between the datasets of Lago *et al.*[8] and McLinden and Perkins.[9] The new equation represents the data of McLinden and Perkins[9] with an average deviation of 0.054 %, and 74 % of the total data points are represented within their experimental uncertainties (0.034–0.45 %). Some data points at temperatures above 400 K show deviations over 0.5 % due to larger experimental uncertainties near the critical point. If they are excluded, the average deviation decreases to 0.041 %. The data of Lago *et al.*[8] show systematic negative deviations down to −0.69 %. At pressures above 10 MPa, the deviations tend to be smaller, but rise to 0.15–0.20 % at the highest pressure (35 MPa).

The two datasets for the vapor-phase sound speeds (Mondéjar *et al.*[3] and Kano *et al.*[11]) are nearly consistent. The overall average deviation is 0.084 % for a total of 191 data points included in the two datasets. For the data of Mondéjar *et al.*,[3] deviations at temperatures above 350 K are comparable to the experimental uncertainties (less than 0.04 %), but those at lower temperatures are sometimes larger than the uncertainties. The average deviation is 0.089 %. Kano *et al.*[11] roughly estimated the experimental uncertainty in their sound speed data as less than 0.1 %. The new equation represents the data of Kano *et al.*[11] almost within this uncertainty; the average deviation is 0.064 %.

Liu and Zhao[10] measured the isobaric heat capacity in the liquid phase. The data were not employed during the fitting because of their larger experimental uncertainties (0.81–1.86 %), and because they are less consistent with the (p, ρ, T) and sound speed data in the liquid phase. The average deviation from calculated values is 4.53 %.

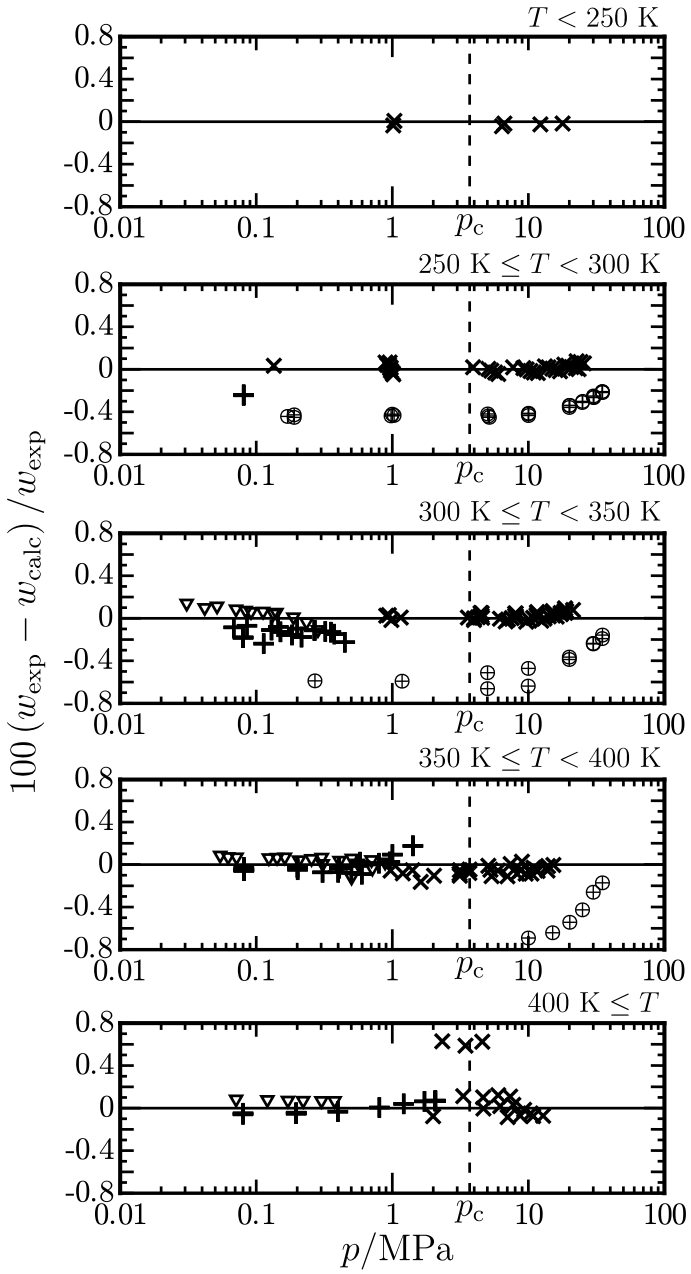

FIG. 8. Relative deviations in the experimental sound-speed data for R1233zd(E): (+) Mondéjar *et al.*[3] (vapor); ($\oplus$) Lago *et al.*[8] (liquid); ($\times$) McLinden and Perkins[9] (liquid); ($\triangledown$) Kano *et al.*[11] (vapor).

3.4. Behavior in the critical and extrapolated regions

Various plots of constant-property lines on several thermodynamic coordinates are shown here to demonstrate the reasonable behavior of the new equation of state in the critical region or in regions away from the experimental data.

Virial coefficients are the most elemental properties related to the interaction potential between molecules, and even without experimental data for the virial coefficients, equations of state should represent their behavior qualitatively. This work constrained the value, slope, and curvature of the second, third, and fourth virial coefficients (B, C, and D) during the fitting. Figure 9 shows values of $(Z-1)/\rho$ calculated from the new equation of state along isotherms in the vapor phase. If these values are plotted versus density, the y intercept (zero density) of each isotherm corresponds to the second virial coefficient B at a given temperature, and the slope at zero density is equal to the third virial coefficient C. All isotherms are very smooth, and no physically incorrect behavior is observed. Values of B, C, and D can be directly calculated from equations of state as follows:

$$B = \lim_{\delta \to 0} \left[\frac{1}{\rho_c} \left(\frac{\partial \alpha^r}{\partial \delta} \right)_\tau \right], \tag{26}$$

$$C = \lim_{\delta \to 0} \left[\frac{1}{\rho_c^2} \left(\frac{\partial^2 \alpha^r}{\partial \delta^2} \right)_\tau \right], \tag{27}$$

and

$$D = \lim_{\delta \to 0} \left[\frac{1}{2\rho_c^3} \left(\frac{\partial^3 \alpha^r}{\partial \delta^3} \right)_\tau \right]. \tag{28}$$

Figure 10 shows plots of B, C, and D versus temperature. Thol *et al.*[42] demonstrated the theoretically expected changes in the virial coefficients based on the analysis of an equation of state for the Lennard-Jones fluid; B and C should go to negative infinity at zero temperature, pass though zero at a moderate temperature, increase to a maximum, and then approach zero at extremely high temperatures. The general trend in D is slightly different from those of B and C at temperatures higher than the first maximum; there should be a second maximum that is smaller in magnitude than the first maximum; after that, D should also decrease to zero at very high temperatures. The behavior of B, C, and D observed in Fig. 10 is in accord with the expected behavior. The inflection point in C is about 3000 K, and this also appears in the equation of state for the Lennard-Jones fluid.

Figures 11 and 12 demonstrate physically correct extrapolation of the new equation of state to regions far from the experimental data. Figure 11 shows the temperature–density behavior

along isobars over wide ranges of temperature and pressure. The saturation boundary and all isobars are very smooth. The rectilinear diameter is straight as it approaches the critical point; this helps to ensure that the saturated vapor densities calculated with the new equation of state are reliable even though the experimental data were not used while fitting. Figure 12 indicates that the extrapolation behavior to extremely high temperatures, pressures, and densities is reasonable. As shown by Lemmon and Jacobsen,[38] the smooth behavior at extreme conditions comes from the first polynomial term with $t_i = 1$ and $d_i = 4$ (the term with the largest d_i in the polynomial terms).

Figure 13 confirms the extrapolation behavior from a different aspect. This figure depicts four characteristic curves on a reduced p-T diagram. Their definitions are given in Table VI. All curves exhibit smooth shapes over wide ranges of temperature and pressure, and no unrealistic bumps are observed.

TABLE VI. Definitions of the four characteristic curves.

Designation	Definition
Ideal curve	$Z = 1$
Boyle curve	$\left(\frac{\partial Z}{\partial \rho}\right)_T = 0$
Joule-Thomson inversion curve	$\left(\frac{\partial Z}{\partial T}\right)_p = 0$
Joule inversion curve	$\left(\frac{\partial Z}{\partial T}\right)_\rho = 0$

Reasonable behavior in the critical region is verified in Figures 14 and 15. Figure 14 plots the saturation boundary in the vicinity of the critical point on a T-ρ diagram, as well as the critical isobar. The saturated liquid and vapor lines smoothly curve and meet at the critical point, and the rectilinear diameter remains straight up to the critical point. In Figure 15, the saturation boundary is plotted on a p-ρ diagram, as well as several isotherms, including the critical isotherm. The isotherms for temperatures below T_c should have only two intersections with the saturation boundary; this suggests that the Maxwell criteria has a single solution at a given temperature. The critical isotherm should exhibit a zero slope and zero inflection in the slope at the critical point,

$$\left(\frac{\partial p}{\partial v}\right)_{T=T_c} = 0 \tag{29}$$

and

$$\left(\frac{\partial^2 p}{\partial v^2}\right)_{T=T_c} = 0. \tag{30}$$

Applying Eqs. (29) and (30) to the new equation of state, the critical temperature and density are calculated as

$$T_{c,calc} = 438.86000\ \text{K} \quad \text{and} \quad \rho_{c,calc} = 3.7040000\ \text{mol dm}^{-3}. \tag{31}$$

These values are almost exactly the same as the critical temperature and density used as the reducing parameters due to additional digits in the coefficients of the third and fourth terms of the polynomial terms.

The behavior of derived properties in the critical and extrapolated regions were also constrained while fitting. Figure 16 shows the residual isochoric heat capacities c_v^r ($= c_v - c_v^\circ$) versus temperature along the saturation lines, isobars, and the critical isochore. The critical isochore is the line from the critical point to higher temperatures with a density equal to the critical density. Figure 17 depicts the residual isobaric heat capacities c_p^r ($= c_p - c_p^\circ$) versus temperature along the saturation lines and isobars over a broader range of temperature. These figures demonstrate reasonable behavior of the new equation of state not only within the range of the experimental data, but also for extrapolated states at higher temperatures and pressures, and lower temperatures. The very steep positive gradients in c_v^r along the saturation lines in the critical region come from the last two Gaussian terms. The critical isochore monotonically decreases from the critical point to higher temperatures, which means that temperature derivatives of the residual Helmholtz energy are properly correlated because the isochoric heat capacity is calculated only from the second partial derivative of the Helmholtz energy with respect to temperature. An upward trend in c_p^r is observed in the liquid region at low temperatures below 200 K. This is common among accurate equations, e.g., the equation for nitrogen[43] and that for propane;[15] however, this cannot be proved experimentally for R1233zd(E) because this occurs below the triple-point temperature (165.75 K). Figure 18 shows the sound speed w versus temperature along the saturation lines and isobars. The saturated liquid line in this figure is a smooth arc when displayed on a logarithmic scale, and there is no physically incorrect behavior over wide ranges of temperature and pressure.

The phase identification parameter (PIP),[40] which was originally used to distinguish whether a state point is in the vapor or liquid phase, has often been used to inspect the behavior of the equation. The PIP can highlight incorrect behavior in an equation of state, since it is calculated

from higher-order derivatives of the Helmholtz energy. The PIP is defined as

$$\mathrm{PIP} = 2 - \rho \left[\frac{\dfrac{\partial^2 p}{\partial \rho \partial T}}{\left(\dfrac{\partial p}{\partial T}\right)_\rho} - \frac{\left(\dfrac{\partial^2 p}{\partial \rho^2}\right)_T}{\left(\dfrac{\partial p}{\partial \rho}\right)_T} \right]. \tag{32}$$

Figure 19 shows the PIP versus temperature along isobars from 0.5 MPa to 1000 MPa, and Figure 20 depicts the PIP versus density along isotherms from 100 K to 5000 K. The saturation lines, isobars, and isotherms are smooth over wide ranges of temperature and pressure, and no unreasonable behavior is observed.

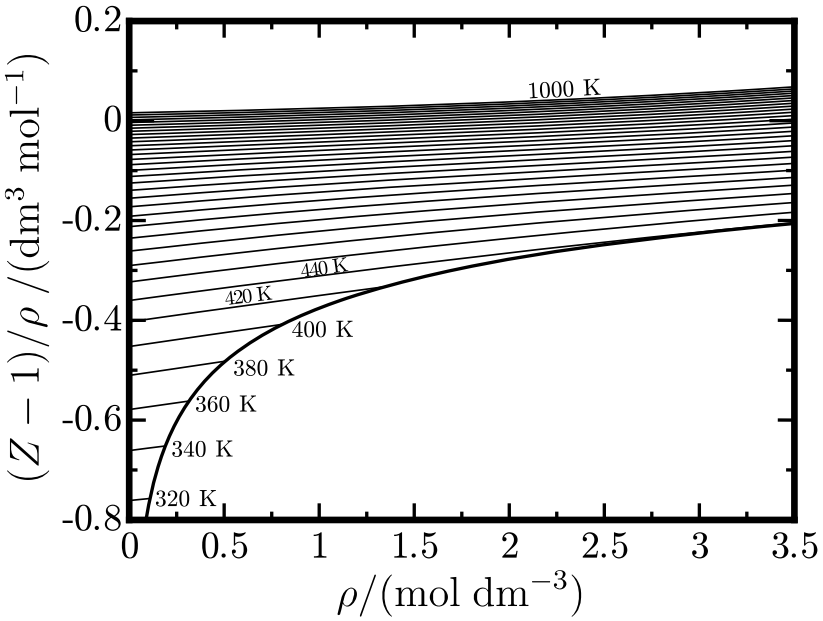

FIG. 9. Values of $(Z - 1)/\rho$ calculated from the equation of state along isotherms in the vapor phase. Isotherms are shown between 320 K and 1000 K with an interval of 20 K.

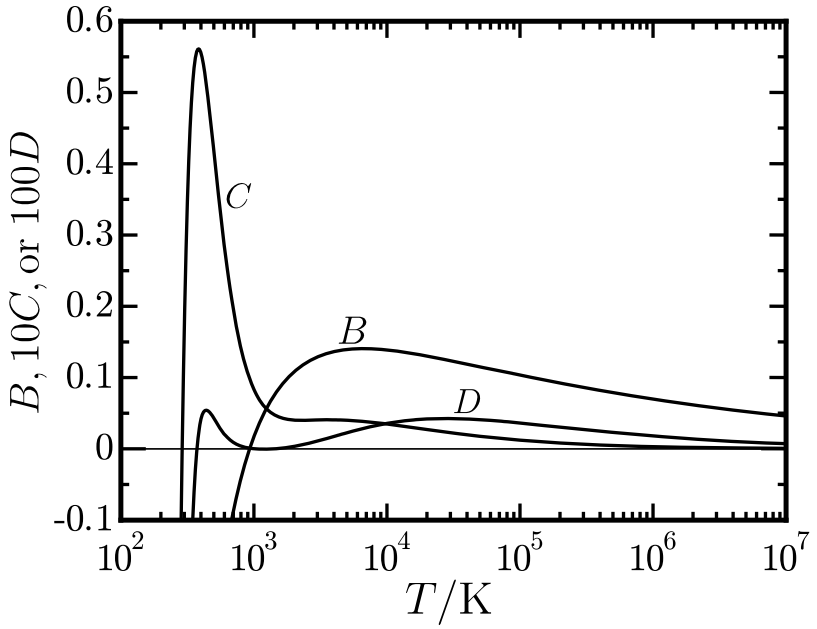

FIG. 10. Second, third, and fourth virial coefficients (B, C, and D) versus temperature. In this plot, the values along the y-axis are equal to the value of B, the value of $10\,C$, and the value of $100\,D$. The units of B, C, and D are ($\mathrm{dm^3\ mol^{-1}}$), ($\mathrm{dm^6\ mol^{-2}}$), and ($\mathrm{dm^9\ mol^{-3}}$), respectively.

.

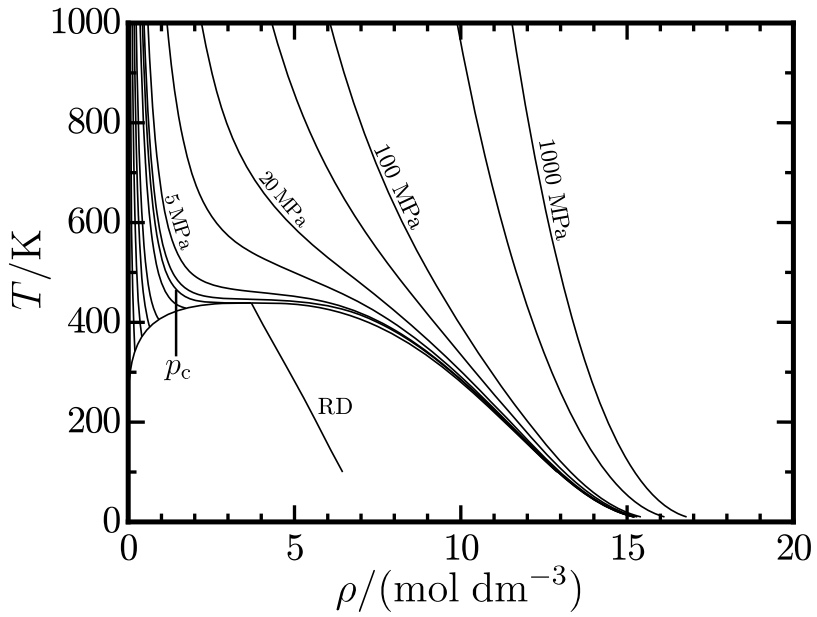

FIG. 11. Temperature versus density along isobars at 0.1, 0.5, 1, 1.5, 2, 3, p_c, 4, 5, 10, 20, 50, 100, 500, and 1000 MPa. RD: Rectilinear diameter.

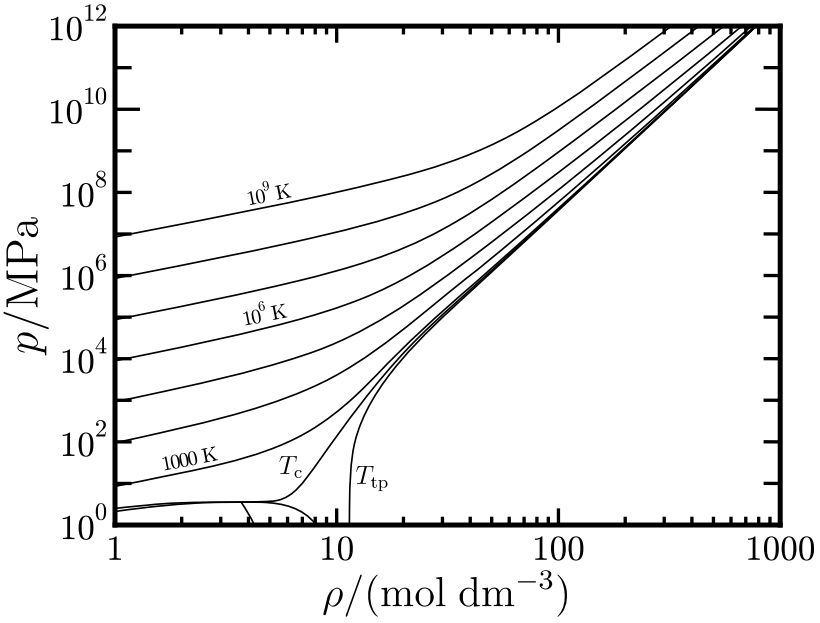

FIG. 12. Pressure versus density along isotherms at T_{tp}, T_c, 10^3, 10^4, 10^5, 10^6, 10^7, 10^8, and 10^9 K.

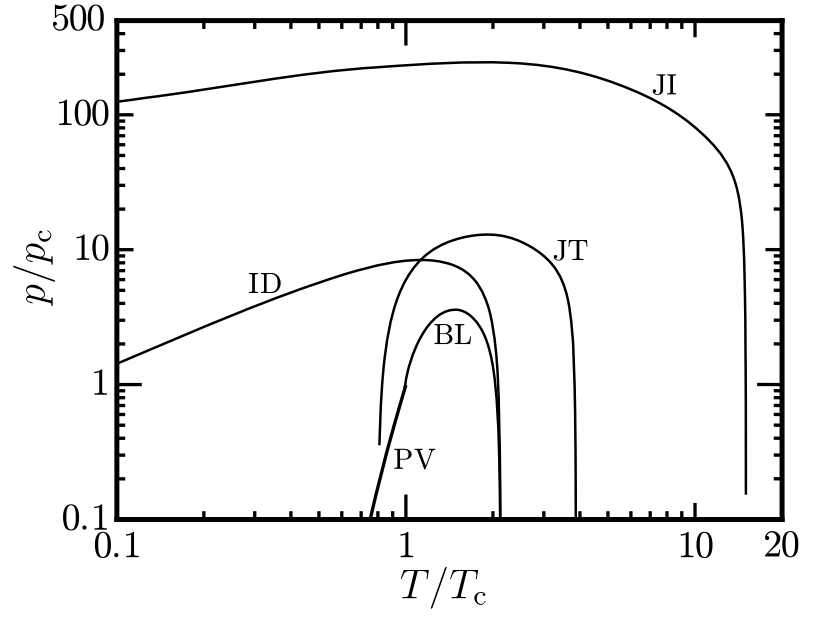

FIG. 13. Four characteristic curves and the vapor pressure curve (PV). ID: ideal curve; BL: Boyle curve; JT: Joule-Thomson inversion curve; JI: Joule inversion curve.

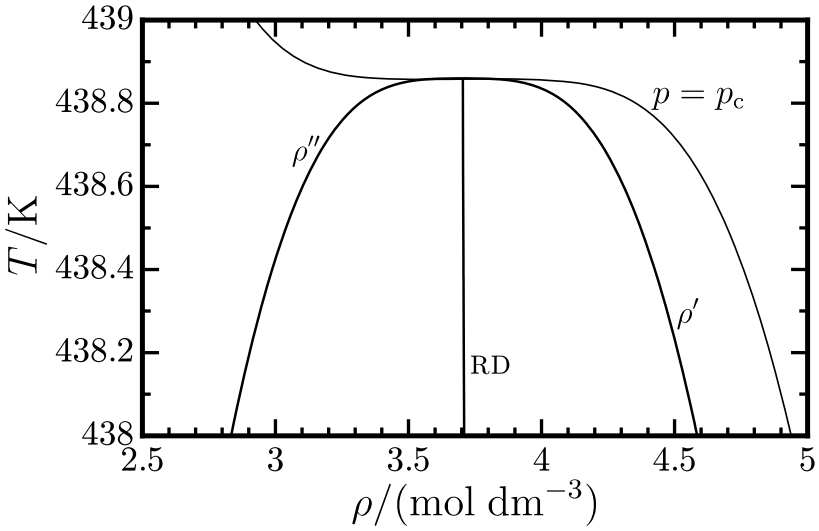

FIG. 14. Saturation boundary and critical isobar ($p = p_c$) in the vicinity of the critical point. RD: Rectilinear diameter.

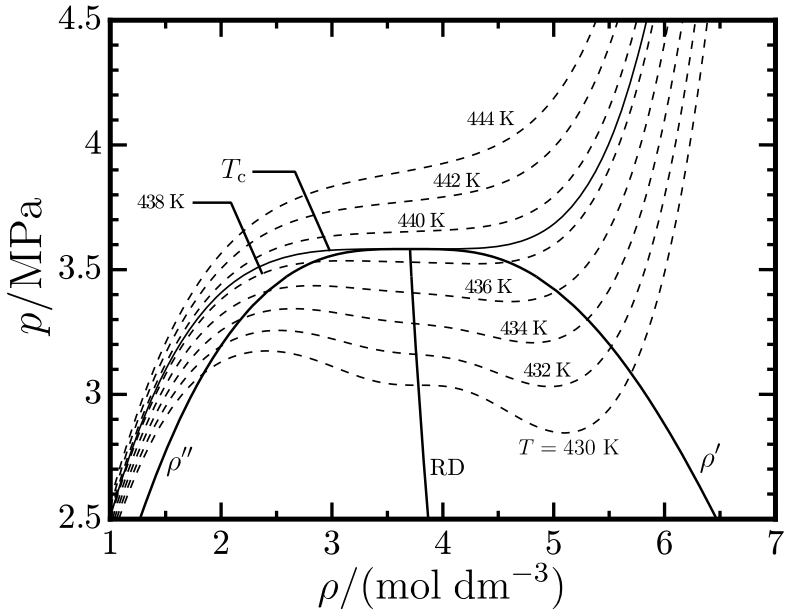

FIG. 15. Saturation boundary and several isotherms, including the critical isotherm ($T = T_c$). RD: Rectilinear diameter.

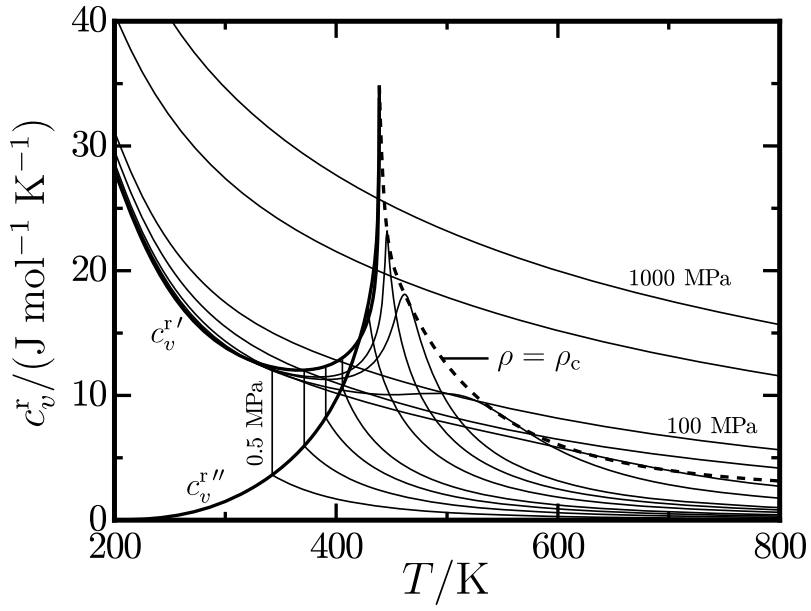

FIG. 16. Residual isochoric heat capacity (c_v^{r}) versus temperature along isobars at 0.5, 1, 1.5, 2, 3, 4, 5, 10, 20, 50, 100, 500, and 1000 MPa, and the critical isochore ($\rho = \rho_{\mathrm{c}}$).

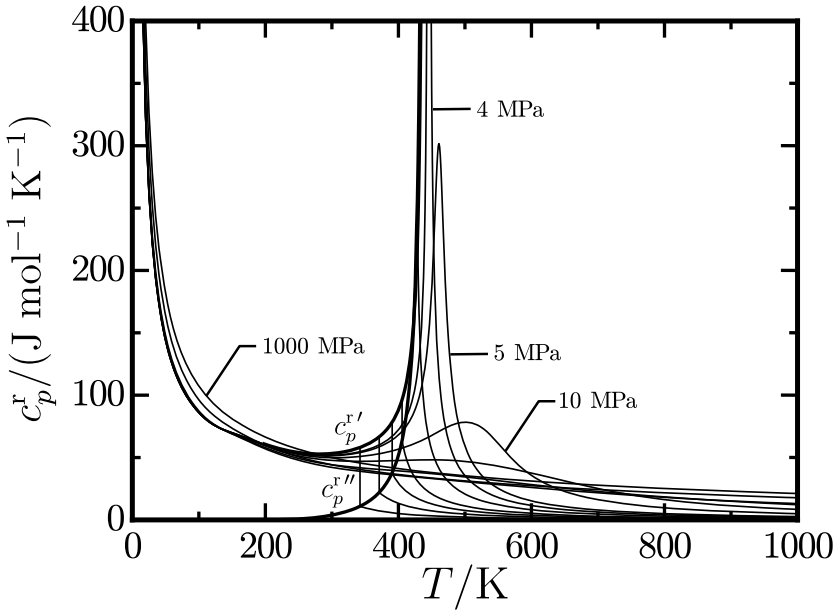

FIG. 17. Residual isobaric heat capacity (c_p^{r}) versus temperature along isobars at 0.5, 1, 1.5, 2, 3, 4, 5, 10, 20, 50, 100, 500, and 1000 MPa.

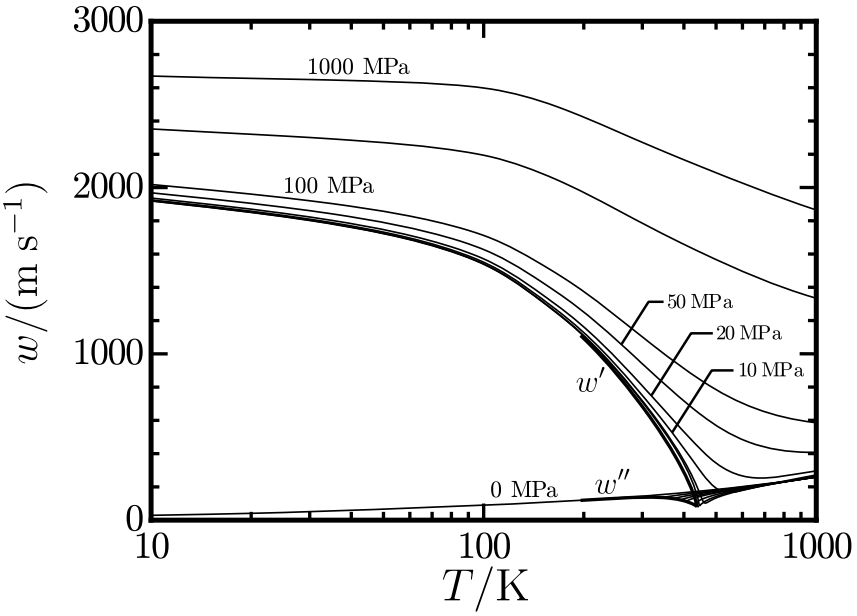

FIG. 18. Sound speed (w) versus temperature along isobars at 0, 0.5, 1, 1.5, 2, 3, 4, 5, 10, 20, 50, 100, 500, and 1000 MPa.

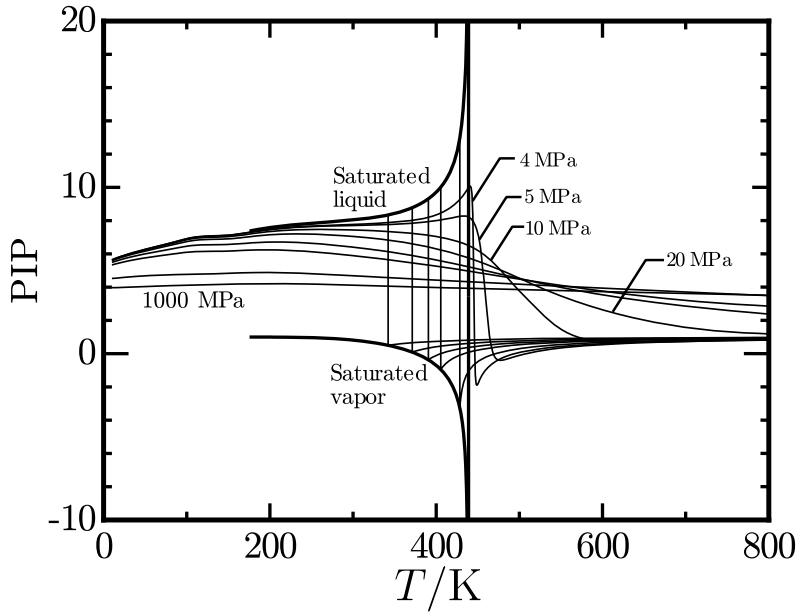

FIG. 19. Phase identification parameter versus temperature along isobars at 0.5, 1, 1.5, 2, 3, 4, 5, 10, 20, 50, 100, 500, and 1000 MPa.

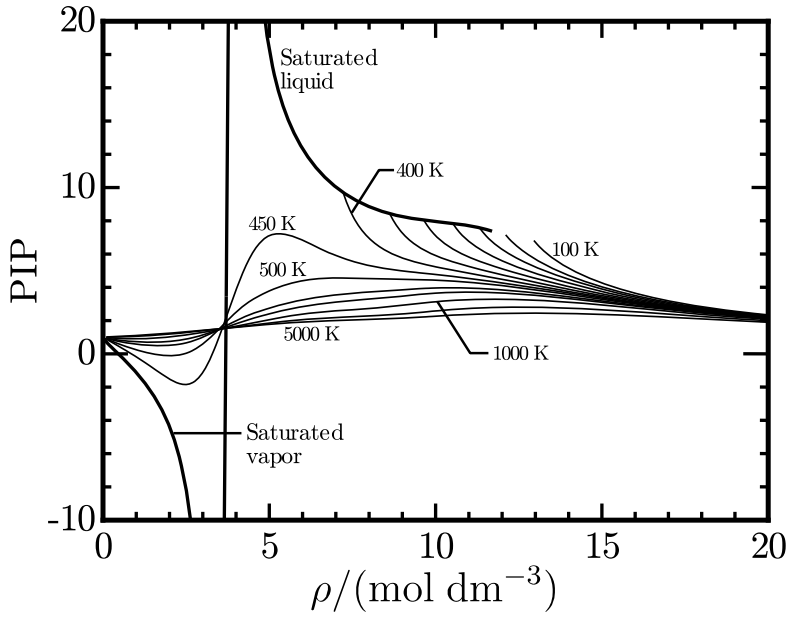

FIG. 20. Phase identification parameter versus density along isotherms at 100, 150, 200, 250, 300, 350, 400, 450, 500, 600, 700, 1000, 2000, and 5000 K.

3.5. Ancillary equations

Ancillary equations are presented for the vapor pressure and saturated liquid and vapor densities. These equations were formulated based on calculated values with the final equation of state. They provide rapid calculations of very close estimates of the saturation properties and give excellent initial guesses for the iterative process to find rigorous solutions for the saturation state from the full equation of state based on the Maxwell criterion. The equations presented here meet the requirements for the ancillary equations stated by Lemmon and Goodwin[44] and Gao *et al.*[19] Coefficients n_i of each equation are given in Table VII.

The vapor pressure p_s is correlated with the equation

$$\ln\left(\frac{p_s}{p_c}\right) = \frac{T_c}{T}\left(n_1\theta + n_2\theta^{1.5} + n_3\theta^{2.39} + n_4\theta^{4.53}\right), \tag{33}$$

where T_c and p_c are the critical temperature (438.86 K) and pressure (3.5828 MPa), and $\theta = 1 - T/T_c$. The saturated liquid and vapor densities (ρ' and ρ'') are represented as

$$\frac{\rho'}{\rho_c} = 1 + n_1\theta^{0.22} + n_2\theta^{0.55} + n_3\theta^{0.94} + n_4\theta^{1.4} + n_5\theta^{6.8}, \tag{34}$$

and

$$\ln\left(\frac{\rho''}{\rho_c}\right) = n_1\theta^{0.24} + n_2\theta^{0.59} + n_3\theta + n_4\theta^{2.2} + n_5\theta^{4.7} + n_6\theta^{9}, \tag{35}$$

where ρ_c is the critical density (3.704 mol dm^{-3}). Average deviations between calculated values with Eqs. (33), (34), and (35) and the rigorous Maxwell solutions with the full equation of state from the triple-point temperature to the critical temperature are 0.0056 %, 0.0081 %, and 0.040 %, respectively.

TABLE VII. Coefficients of Eqs. (33), (34), and (35).

	Eq. (33)	Eq. (34)	Eq. (35)
n_1	−7.4798	0.61448	−0.80785
n_2	1.5791	2.6345	−3.2355
n_3	−1.7959	−1.316	−2.7567
n_4	−3.6716	0.86885	−10.863
n_5		0.34071	−33.456
n_6			−69.31

4. CONCLUSIONS: ESTIMATED UNCERTAINTIES IN CALCULATED PROPERTIES

A new Helmholtz energy equation of state has been developed for R1233zd(E) in this work, which is expressed with temperature and density as independent variables. The experimental data used in the development of the new equation of state are located at temperatures from 215 K to 444 K and pressures up to 35 MPa. In this range, typical uncertainties (expanded uncertainty with a coverage factor of $k = 2$) in calculated properties from the new equation are 0.07 % for vapor pressures at temperatures above the normal boiling point temperature ($\approx$ 291 K), 0.2 % for vapor pressures at lower temperatures, 0.05 % for liquid densities, 0.15 % for vapor densities, 0.1 % for saturated liquid densities, 0.05 % for liquid-phase sound speeds, and 0.08 % for vapor-phase sound speeds. They are tabulated in Table VIII.

Plots of constant-property lines on several thermodynamic coordinates demonstrate that the new equation is capable of successfully extrapolating to higher temperatures and pressures, and to lower temperatures; therefore, we conclude that the new equation is applicable to temperatures from the triple-point temperature (165.75 K) to 450 K and pressures up to 100 MPa with reasonable uncertainties. Uncertainties in the expanded region are larger than the typical uncertainties in the region of experimental data. The new equation of state does not include the effects of dissociation, which begins around 450 K. The thermal stability of R1233zd(E) is discussed in the literature.[45–48]

The new equation of state for R1233zd(E) has been recommended as an international standard formulation by the ISO working group presently revising ISO 17584.[23] As an aid in computer implementation, calculated property values from the new equation of state are given in Table IX. A fluid file (R1233ZDE.FLD) for use in REFPROP[49] and TREND,[50] a fluid file (R1233ZDE.json) for use in CoolProp,[51] and Python code to display the values in Table IX are given in the supplementary material.

TABLE VIII. Typical uncertainties ($k = 2$) in calculated properties from the new equation of state for R1233zd(E).

Range: 215 K $\leq T \leq$ 444 K, $p \leq$ 35 MPa		
Property	Uncertainty	Remark
Vapor pressure	0.07 %	$T > T_b$ (≈ 291 K)
	0.2 %	$T < T_b$
Liquid density	0.05 %	
Vapor density	0.15 %	
Saturated liqiud density	0.1 %	
Liquid-phase sound speed	0.05 %	
Vapor-phase sound speed	0.08 %	

TABLE IX. Calculated property values from the new equation of state for R1233zd(E) to verify computer code.

T (K)	ρ (mol dm^{-3})	p (MPa)	c_v (J mol^{-1} K^{-1})	c_p (J mol^{-1} K^{-1})	w (m s^{-1})
300	0	0	93.7166	102.031	144.257
300	10	18.20558	107.988	150.070	797.711
300	0.05	0.1192035	94.9935	105.252	138.949
400	8	10.79073	122.693	176.124	441.123
400	0.8	1.791900	121.820	171.027	116.943
439	3.8	3.591512	151.871	56925.2	77.5936

5. ACKNOWLEDGMENTS

The authors thank all members of the working group ISO/TC 86/SC 8/WG 7 for their valuable suggestions during the development of the new equations of state. The authors appreciate Mark O. McLinden, National Institute of Standards and Technology, Boulder, and Kehui Gao, Xi'an Jiaotong University, for their assistance during the documentation of this paper, and Ian H. Bell, National Institute of Standards and Technology, Boulder, for his generous support in programming the supplementary computer code.

6. AUTHOR DECLARATIONS

6.1. Conflict of interest

The authors have no conflicts to disclose.

7. DATA AVAILABILITY

Data sharing is not applicable to this article as no new data were created or analyzed in this study.

REFERENCES

[1]K. O. Patten and D. J. Wuebbles, Atmos. Chem. Phys. **10**, 10867 (2010).

[2]G. Myhre, D. Shindell, F.-M. Bréon, W. Collins, J. Fuglestvedt, J. Huang, D. Koch, J.-F. Lamarque, D. Lee, B. Mendoza, T. Nakajima, A. Robock, G. Stephens, T. Takemura, and H. Zhang, *Anthropogenic and Natural Radiative Forcing. In: Climate Change 2013: The Physical Science Basis. Contribution of Working Group I to the Fifth Assessment Report of the Intergovernmental Panel on Climate Change* (Cambridge University Press, Cambridge, United Kingdom and New York, NY, USA, 2013).

[3]M. E. Mondéjar, M. O. McLinden, and E. W. Lemmon, J. Chem. Eng. Data **60**, 2477 (2015).

[4]K. Tanaka, Trans. Japan Soc. Refrig. Air Cond. Eng. **33**, 105 (2016).

[5]R. Romeo, P. A. Giuliano Albo, S. Lago, and J. S. Brown, Int. J. Refrig. **79**, 176 (2017).

[6]L. Fedele, M. Pierantozzi, G. Di Nicola, J. S. Brown, and S. Bobbo, J. Chem. Eng. Data **63**, 225 (2018).

[7]J. Yin, J. Ke, G. Zhao, and S. Ma, Int. J. Refrig. **121**, 253 (2021).

[8]S. Lago, P. A. Giuliano Albo, J. S. Brown, and M. Bertinetti, J. Chem. Eng. Data **63**, 4039 (2018).

[9]M. O. McLinden and R. A. Perkins, submitted to J. Chem. Thermodyn. (2022).

[10]Y. Liu and X. Zhao, Int. J. Refrig. **86**, 127 (2018).

[11]Y. Kano, Y. Kayukawa, and Y. Fujita, Int. J. Refrig. **118**, 354 (2020).

[12]G. Di Nicola, L. Fedele, J. S. Brown, S. Bobbo, and G. Coccia, J. Chem. Eng. Data **62**, 2496 (2017).

[13]S. Li, F. Yang, K. Zhang, Y. Duan, and Z. Yang, J. Chem. Eng. Data **64**, 2947 (2019).

[14]N. Sakoda, Y. Higashi, and R. Akasaka, J. Chem. Eng. Data **65**, 4285 (2020).

[15]E. W. Lemmon, M. O. McLinden, and W. Wagner, J. Chem. Eng. Data **54**, 3141 (2009).

[16]M. Thol, E. W. Lemmon, and R. Span, High Temp.-High Press. **41**, 81 (2012).

[17]R. Akasaka, Y. Zhou, and E. W. Lemmon, J. Phys. Chem. Ref. Data **44**, 013104 (2015).

[18]M. Thol and E. W. Lemmon, Int. J. Thermophys **37**, 1 (2016).

[19]K. Gao, J. Wu, P. Zhang, and E. W. Lemmon, J. Chem. Eng. Data **61**, 2859 (2016).

[20]S. Herrig, M. Thol, A. H. Harvey, and E. W. Lemmon, J. Phys. Chem. Ref. Data **47**, 043102 (2018).

[21]R. Akasaka and E. W. Lemmon, J. Chem. Eng. Data **64**, 4679 (2019).

[22]ISO Standard 17584:2005 Refrigerant Properties; International Organization for Standardization (2005).

[23]ISO/DIS 17584 Refrigerant Properties; International Organization for Standardization (2022).

[24]R. J. Hulse, R. S. Basu, R. R. Singh, and R. H. P. Thomas, J. Chem. Eng. Data **57**, 3581 (2012).

[25]G. Raabe, J. Chem. Eng. Data **60**, 2412 (2015).

[26]G. Raabe, J. Chem. Eng. Data **65**, 1234 (2020).

[27]K. Tanaka, J. Chem. Eng. Data **61**, 3570 (2016).

[28]K. Tanaka and R. Akasaka, Int. J. Refrig. **131**, 61 (2021).

[29]S. Tomassetti, G. Di Nicola, and C. Kondou, Int. J. Refrig. **133**, 172 (2022).

[30]E. Tiesinga, P. J. Mohr, D. B. Newell, and B. N. Taylor, J. Phys. Chem. Ref. Data **50**, 033105 (2021).

[31]H.-J. Kretzschmar, T. Zschunke, J. Klinger, and A. I. Dittman, in *Proceedings of The 11th International Conference on Properties of Water and Steam* (Hemisphere, NY, USA, 1990).

[32]R. Span, *Multiparameter Equations of State: An Accurate Source of Thermodynamic Property Data* (Springer Berlin, 2000).

[33]R. Akasaka, J. Therm. Sci. Technol. **3**, 442 (2008).

[34]D. A. McQuarrie, *Statistical Mechanics, Chapter 8* (Harper & Row, 1975).

[35]Y. Kano, unpublished data (2020).

[36]M. J. Frisch, G. W. Trucks, H. B. Schlegel, G. E. Scuseria, M. A. Robb, J. R. Cheeseman, G. Scalmani, V. Barone, B. Mennucci, G. A. Petersson, H. Nakatsuji, M. Caricato, X. Li, H. P. Hratchian, A. F. Izmaylov, J. Bloino, G. Zheng, J. L. Sonnenberg, M. Hada, M. Ehara, K. Toyota, R. Fukuda, J. Hasegawa, M. Ishida, T. Nakajima, Y. Honda, O. Kitao, H. Nakai, T. Vreven, J. A. Montgomery, Jr., J. E. Peralta, F. Ogliaro, M. Bearpark, J. J. Heyd, E. Brothers, K. N. Kudin, V. N. Staroverov, R. Kobayashi, J. Normand, K. Raghavachari, A. Rendell, J. C. Burant, S. S. Iyengar, J. Tomasi, M. Cossi, N. Rega, J. M. Millam, M. Klene, J. E. Knox, J. B. Cross, V. Bakken, C. Adamo, J. Jaramillo, R. Gomperts, R. E. Stratmann, O. Yazyev, A. J. Austin, R. Cammi, C. Pomelli, J. W. Ochterski, R. L. Martin, K. Morokuma, V. G. Zakrzewski, G. A. Voth, P. Salvador, J. J. Dannenberg, S. Dapprich, A. D. Daniels, O. Farkas, J. B. Foresman, J. V. Ortiz, J. Cioslowski, and D. J. Fox, Gaussian 09 Revision D.01 (2009), Gaussian Inc. Wallingford CT 2009.

[37]K. K. Irikura, R. D. Johnson 3rd, and R. N. Kacker, J. Phys. Chem. A **109**, 8430 (2005).

[38]E. W. Lemmon and R. T. Jacobsen, J. Phys. Chem. Ref. Data **34**, 69 (2005).

[39]R. Span and W. Wagner, Int. J. Thermophys. **18**, 1415 (1997).

[40]G. Venkatarathnam and L. R. Oellrich, Fluid Phase Equilib. **301**, 225 (2011).

[41]R. Akasaka, Y. Higashi, N. Sakoda, S. Fukuda, and E. W. Lemmon, Int. J. Refrig. **119**, 457 (2020).

[42]M. Thol, G. Rutkai, A. Köster, R. Lustig, R. Span, and J. Vrabec, J. Phys. Chem. Ref. Data **45**, 023101 (2016).

[43]R. Span, E. W. Lemmon, R. T. Jacobsen, W. Wagner, and A. Yokozeki, J. Phys. Chem. Ref. Data **29**, 1361 (2000).

[44]E. W. Lemmon and A. R. H. Goodwin, J. Phys. Chem. Ref. Data **29**, 1 (2000).

[45]J. R. Juhasz and L. D. Simoni, in *Proceedings of 3rd International Seminar on ORC Power Systems* (Brussels, Belgium, 2015).

[46]J. Majurin, E. Sorenson, D. Steinke, and M. Herried, in *Proceedings of 2017 ASHRAE Winter Conference* (Las Vegas, NV, USA, 2017).

[47]S. Kim, W. Rached, and L. Abbas, in *Proceedings of the 17th International Refrigeration and Air Conditioning Conference* (West Lafayette, IN, USA, 2018).

[48]C. Mateu-Royo, J. Navarro-Esbrí, A. Mota-Babiloni, M. Amat-Albuixech, and F. Molés, Appl. Therm. Eng. **152**, 762 (2019).

[49]E. W. Lemmon, I. H. Bell, M. L. Huber, and M. O. McLinden, NIST Standard Reference Database 23: Reference Fluid Thermodynamic and Transport Properties-REFPROP, Version 10.0, National Institute of Standards and Technology (2018).

[50]R. Span, R. Beckmüller, S. Hielscher, A. Jäger, E. Mickoleit, T. Neumann, S. Pohl, B. Semrau, and M. Thol, TREND. Thermodynamic Reference and Engineering Data 5.0. Lehrstuhl für Thermodynamik, Ruhr-Universität Bochum (2020).

[51]I. H. Bell, J. Wronski, S. Quoilin, and V. Lemort, Ind. Eng. Chem. Res. **53**, 2498 (2014).